ÍNDICE

A SYSTEM FOR MULTILOOK POLARIMETRIC SAR IMAGE STATISTICAL CLASSIFICATION•

Corina da Costa Freitas [1]
Antonio Henrique Correia [1]
Alejandro C. Frery [2]
Sidnei J. S. Sant'Anna [1]

[1] INPE - Instituto Nacional de Pesquisas Espaciais
DPI - Divisão de Processamento de Imagens
Avenida dos Astronautas, 1758
12227-010 São José dos Campos, SP, Brasil
correia,corina,sidnei@dpi.inpe.br

[2] UFPE - Universidade Federal de Pernambuco
DI - Departamento de Informática
CP 7851
50732-970 Recife, PE, Brasil
frery@di.ufpe.br

Abstract. This paper presents a system for the statistical classification of multilook polarimetric SAR images. The methods used are the pointwise Maximum Likelihood (ML), as initial solution, and the contextual ICM (*Iterated Conditional Modes*) algorithm. The multilook SAR data are modelled from the multivariate complex Wishart distribution, and the densities for several important transformations are derived. The system is user-friendly, since it is based upon interactive graphic user interfaces. With this approach, the statistical modelling is hidden to the user. Examples of classifications of SIR-C/X-SAR images is presented.

Keywords: classification, context, ICM, multilook polarimetric SAR, statistics.

1 INTRODUCTION

The intensification of remote sensing studies in the field of Synthetic Aperture Radar (SAR) imaging sensors is leading towards a better understanding of the scattering mechanisms of terrestrial targets in the microwaves spectrum. Besides this, it has led to more dependable applications of SAR imagery and products to geology, cartography, and other fields of knowledge.

One of the most useful products of digital images is the result of automatic or semiautomatic data classification. This product is becoming more and more precise since the Gaussian hypothesis

• This work was supported by grants from PPG-7 (0808/95 and 0816/95), Convênio FINEP (6.6.96.0473.00 and 6.6.96.0474.00).

was weakened, and since better suited distributions were incorporated into the process (Nezry et al., 1996; Frery et al., 1997a).

In Vieira (1996) this improvement becomes evident: it is shown that the simultaneous use of proper distribution for each class, along with contextual information, leads to better classifications than those obtained either by Gaussian fitting and/or pointwise classification. On the other hand, the use of single-band SAR data has its limitations.

The number of studies and applications involving polarimetric SAR data is increasing steadily. These data are formed by sending and receiving the electromagnetic signal in both horizontal and vertical polarisation and, thus, they may carry a larger amount of information than that available from a single band. Though there is currently no sensor operating in different bands and polarisations, studies in this area are useful.

Several works are devoted to the statistical characterisation of single-look polarimetric SAR data. The reader is referred to DeGrandi et al. (1992), Kong, (1988), Lim et al. (1989), Quegan and Rhodes (1995), Yueh et al. (1989), to name a few.

The potential of multilook polarimetric data, where each value is the mean over several observations, is notorious as presented in Lee and Grunes (1994) and in Lee et al. (1995), for instance. The statistical properties of this kind of data have not been fully exploited yet. They have the advantage of exhibiting a speckle noise reduction as well as data reduction.

A system for multilook polarimetric SAR image classification was developed, in order to assess the potential of this kind of data. It is strongly based on the statistical properties of the data, and it uses a ML classification as the initial configuration for a contextual Markovian classification technique: the ICM, presented in Vieira (1996). In this work an extension of this system is presented, which allows the analysis of intensity, phase difference, ratio of intensities and intensity-phase data. These data formats are derived from multilook polarimetric SAR imagery, and their distributional properties are here recalled. The system if based on graphic user interfaces, and was developed as an extension of the ENVI image processing system.

2 POLARIMETRIC SAR SYSTEMS

Conventional SAR systems operate in a single frequency, with a single antenna of fixed polarisation for both the transmitted and received signals. Either the intensity or the amplitude of the returned signal is recorded and, as a consequence, any information carried in the phase of the complex electromagnetic signal is lost.

When polarimetric SAR sensors are used, the full complex signal is recorded and, thus, the return in all the configurations (*HH*, *HV*, *VH* and *VV*) are fully recorded (intensities and relative phases). In order to accomplish this for every resolution cell the complex scattering matrix, denoted as

$$\boldsymbol{S} = \begin{pmatrix} S_{VV} & S_{VH} \\ S_{HV} & S_{HH} \end{pmatrix} \tag{1}$$

is measured. Subscripts $p, q \in \{H, V\}$ denote the transmission and emission components of the signal, respectively, and elements S_{pq} are called *complex scattering amplitude*. Sarabandi (1992) shows that

$$S_{pq} = \left|S_{pq}\right| e^{if_{pq}} = \sum_{n=1}^{N} \left|s_{pq}^{n}\right| e^{if_{pq}^{n}}, \tag{2}$$

where N is the number of scatterers of each resolution element, each having amplitude $\left|s_{pq}^{n}\right|$ and phase f_{pq}^{n}.

Other ways of representing polarimetric data are the Stokes matrix, the modified Stokes matrix, the covariance matrix and the Mueller matrix (Ulaby and Elachi, 1990).

3 STATISTICAL PROPERTIES OF POLARIMETRIC SAR DATA

Data obtained with coherent illumination, as is the case of SAR data, are corrupted by a signal-dependent noise called *speckle*. A usual model for the signal and this noise is the Multiplicative Model. It states that, under certain conditions (Tur et al., 1982) the observed value in every pixel is the outcome of the random variable $Z = XY$, where X is the random variable that models the *backscatter* and Y is the one that models the *speckle* noise, and these last two are independent.

Statistical models for multilook polarimetric data are derived from the covariance matrix, which exhibits a complex Wishart distribution (Lee and Grunes, 1992; Du and Lee,1996).

Ulaby and Elachy (1990) show that, for satellites that transmit and receive through the same antenna (which is the usual case), it is possible to suppose that $S_{HV} = S_{VH}$. Therefore, the matrix presented in **eq. (1)** can be reduced, without loss of information to

$$\boldsymbol{Z} = \begin{bmatrix} S_1 \\ S_2 \\ S_3 \end{bmatrix}, \tag{3}$$

where S_i, $1 \le i \le 3$ denotes S_{HH}, S_{HV} and S_{VV} in any convenient order.

When the number of elementary backscatterers (denoted N in **eq. (2)**) is very large, it can be assumed that the vector $\boldsymbol{Z}$ in **eq. (3)** obeys a multivariate complex Gaussian distribution (Goodman, 1963). This is true if the backscatter X is constant, independently of the imaged area, since the speckle Y is assumed to obey a multivariate complex Gaussian law.

In this work multilook data are considered and, in order to derive their distributional properties, vector $\boldsymbol{Z}$ in **eq. (3)** will be, thus, considered the k-th single-look observation and denoted $\boldsymbol{Z}(k)$. A fixed number, n, of independent outcomes of $\boldsymbol{Z}$ are averaged to form the n-looks covariance matrix, given by (Lee et al., 1995)

$$\boldsymbol{Z}^{(n)} = \frac{1}{n} \sum_{k=1}^{n} \boldsymbol{Z}(k) \boldsymbol{Z}^{*}(k)^{T}, \tag{4}$$

where $\boldsymbol{Z}^{*}(k)^{T}$ denotes the transposed conjugate of $\boldsymbol{Z}(k)$.

The advantage of working with the covariance matrix, defined as $\boldsymbol{A} = n\boldsymbol{Z}^{(n)}$, is that it exhibits a multivariate complex Wishart distribution (Srivastava, 1963). Its density is given by

$$p_{\boldsymbol{Z}^{(n)}}(\boldsymbol{z}) = \frac{n^{qn} \left|\boldsymbol{z}\right|^{(n-q)} \exp[-n\mathrm{Tr}(\boldsymbol{C}^{-1}\boldsymbol{z})]}{K(n,q)\left|\boldsymbol{C}\right|^{n}}, \tag{5}$$

where q denotes the dimension of the vector $\boldsymbol{Z}$, $K(n,q) = p^{\,q\,(q\,-1)/2}\Gamma(n)\cdots\Gamma(n-q+1)$, Tr denotes the trace of the matrix, $\boldsymbol{C} = \mathrm{E}[\boldsymbol{Z}\boldsymbol{Z}^{*T}]$, and Γ is the Euler Gamma function (DeGroot, 1968).

Using **eq. (5)** it is possible to derive the densities for situations of particular interest, as presented in Lee et al. (1995). The following situations were implemented in the system here considered: a pair of intensities, phase difference, ratio of intensities and pair intensity-phase.

4 THE SYSTEM

The system behaves as an extension of the ENVI v. 2.5 (*Environment for Visualisation of Images*) system, and it uses its functions and others from IDL (*Interactive Data Language*). In this manner, several functions such as those for data management, processing and analysis were reused.

Both classifications implemented are supervised and, thus, require the specification of training sets for parameter estimation. These sets are informed through *regions of interest*, previously defined by the used with ENVI utilities. The equivalent number of looks (n in **eqs. (4) and (5)**) is also an input parameter; it can be estimated within the system as presented in Vieira (1996).

The ICM classification method is a contextual procedure that, in order to classify every pixel, uses both the observed value in the corresponding coordinate and the classification of the surrounding sites. In order to incorporate this context within a statistical framework, a Markovian model is incorporated for the classes. This model is known in the literature as Potts-Strauss (Frery et al. 1997b; Vieira, 1996; Vieira et al. 1997).

The system here presented uses an inference technique called *pseudolikelihood*, in order to estimate the required parameters of the Markovian model without the need of intervention of the user. Details are available in Vieira (1996), Vieira et al. (1997) and in Frery et al. (1997b). The current implementation uses any existing classification as starting point, being the ML the preferred one.

The following subsections describe the functionality of the system, in every case for n looks intensity data. The densities and parameter estimators are presented in Lee et al. (1994).

4.1 ICM INTENSITY BIVARIATE SAR

This option applies the ML and ICM classifications to a pair of intensity images, either two polarimetric components or the result of two passages of the same monospectral sensor (such as JERS-1, ERS-1, etc.).

After the input of the initial data the interface shown in **Figure 1** is presented. It exhibits the 2-D histogram of the pair of bands, along with the 2-D estimated density, both in perspective and in contour plot. The estimated parameters are presented at the bottom of the plots. FIG. 1

As every interface presented in this work, that presented in **Figure 1** is fully interactive with the user. The user can specify the interval the plots will be drawn, any desirable rotation, the number of levels to be used, etc. This feature greatly stimulates the interaction of the user with the data. The input values affect all the sub-windows, since they are connected in order to help the visualisation.

This interface has to be used for every class of interest. Once this is performed, the ML classification is performed, and the interface shown in **Figure 2** is presented to the user. The user can interactively choose the classes for which the estimated densities are presented (in perspective and in isolines). The user can specify the viewpoint and number of slices. Each class is associated to a unique colour. FIG. 2

The ML classification is produced, and used as initial configuration by the ICM algorithm. This iterative technique stops according to the number of coordinates whose classification changes from one iteration to the next (Vieira, 1996).

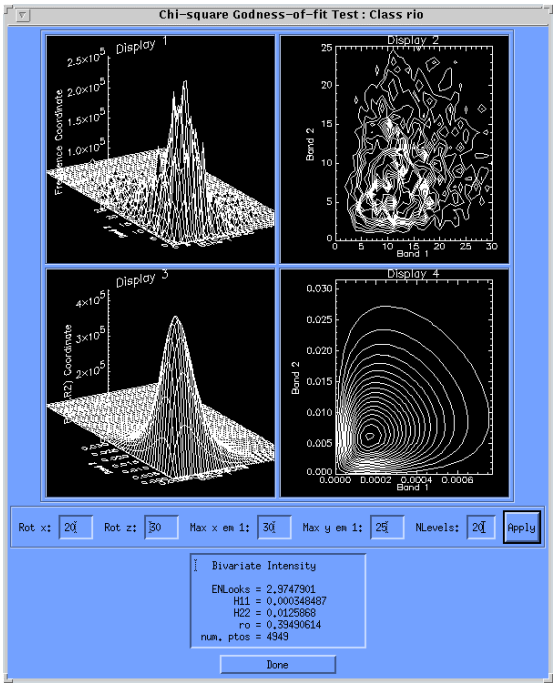

Figure 1 - Density, 2-D histogram, contour plot and estimated parameters of two multilook intensity bands.

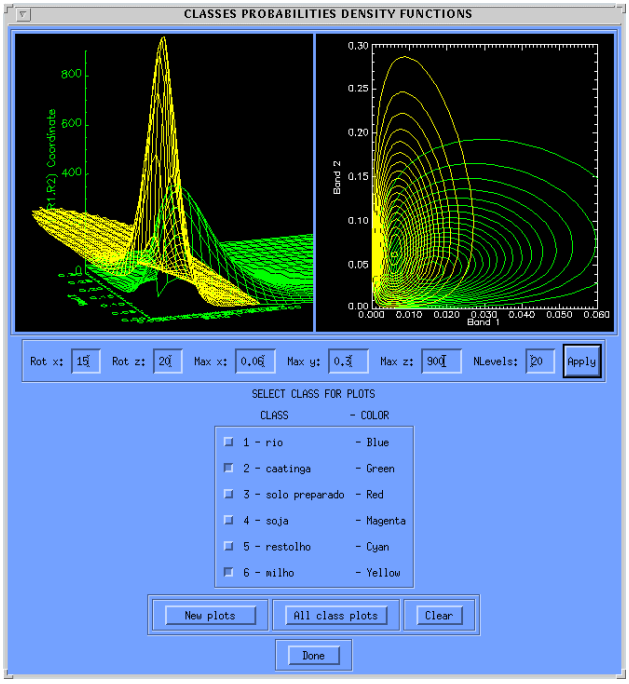

Figure 2 - Densities associated to different classes of interest.

Denoting as R_1, R_2 the pair of intensities, their joint density under the model characterised by **eq. (5)** is

$$p(R_1,R_2)=\frac{n^{n+1}(R_1R_2)^{\frac{(n-1)}{2}}\exp\left(-\dfrac{n\left(\dfrac{R_1}{H_{11}}+\dfrac{R_2}{H_{22}}\right)}{1-|r_c|^2}\right)}{(H_{11}H_{22})^{\frac{(n+1)}{2}}\Gamma(n)(1-|r_c|^2)|r_c|^{n-1}}\,I_{n-1}\left(\frac{2n|r_c|}{1-|r_c|^2}\sqrt{\frac{R_1R_2}{H_{11}H_{22}}}\right),$$

where $H_{11}=\mathrm{E}[R_1]$ and $H_{22}=\mathrm{E}[R_2]$, I_{n-1} denotes the modified Bessel function of order $n-1$, and

$$r_c=\frac{\mathrm{E}[S_iS_j^*]}{\sqrt{\mathrm{E}[|S_i|^2]\mathrm{E}[|S_j|^2]}}=|r_c|e^{iq}$$

The parameter $|r_c|$ can be estimated by

$$\hat{r}=\frac{\mathrm{E}[(R_1-\overline{R}_1)(R_2-\overline{R}_2)]}{\sqrt{\mathrm{E}[(R_1-\overline{R}_1)^2]\mathrm{E}[(R_2-\overline{R}_2)^2]}}$$

Where $\overline{R}_1$ and $\overline{R}_2$ denotes the mean of R_1 and R_2 , respectively.

4.2 ICM PHASE DIFFERENCE SAR

This option applies the ML and ICM classifications to Y, the difference between the phases of two complex images. These images are derived from two components $S_i(k)$ and $S_j(k)$ of single-look images (**eq. (2)**) in the following manner:

$$Y = Arg\left|\overbrace{\frac{1}{n}\sum_{k=1}^{n} S_i(k)S_j^*(k)}^{R_{ij}^{(n)}}\right| = \tan^{-1}\left[\frac{\Im\left[R_{ij}^{(n)}\right]}{\Re\left[R_{ij}^{(n)}\right]}\right] \tag{6}$$

where $\Re$ and $\Im$ denote, respectively, real and imaginary parts.

After the required parameters have been introduced, **Figure 3** is presented, with the histogram of the data, the fitted density and estimated phase difference parameters. When every class has been checked with this interface, **Figure 4** is shown. This interface presents the estimated densities of the phase difference for every considered class, allowing the visual assessment of their separability throughout this feature.

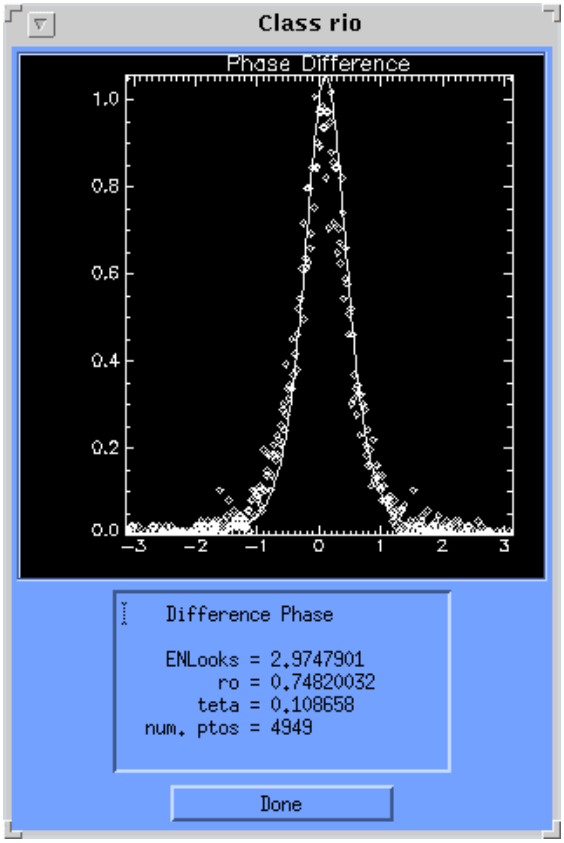

Figure 3 - Histogram, fitted density and estimated phase difference parameters.

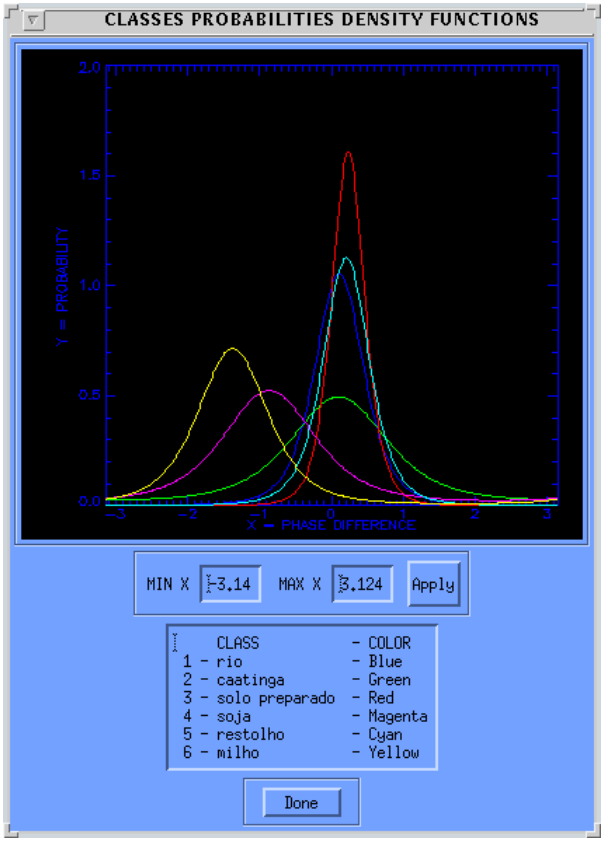

Figure 4 - Estimated densities of the phase difference for every considered class.

The density of the quantity defined above, under the aforementioned model, is given by

$$p_{\Psi}^{(n)}(y) = \frac{\Gamma(n+1/2)(1-|r_c|^2)^n b}{2\sqrt{p}\,\Gamma(n)(1-b^2)^{n+1/2}} + \frac{(1-|r_c|^2)^n}{2p} F(n,1;1/2;b^2) \;\; (-p < y \le p)$$

where $-p < y \le p$, $b = |r_c|\cos(y-q)$, q is the phase of the complex coefficient of correlation and $F(n,1;1/2;b^2) = {}_2F_1(n,1;1/2;b^2)$ is the Gaussian hypergeometric function (Abramowitz and Stegun, 1964).

4.3 ICM RATIO OF INTENSITIES

Both the ML and ICM classification are obtained, derived from the ratio between two multilook intensity bands, i.e., using data of the form R_i/R_j.

Analogously to the previous situation, namely for the classification using phase difference, after the required inputs the histogram, fitted densities and estimated parameters are shown for every class. Once the fittings have been checked for every class, the whole set of fitted densities is shown.

The density that characterises this data is

$$p^{(n)}(w) = \frac{t^n\,\Gamma(2n)(1-|r_c|^2)^n (t+w) w^{n-1}}{\Gamma(n)\Gamma(n)[(t+w)^2 - 4t\,|r_c|^2 w]^{(2n+1)/2}}, \; onde \;\; t = H_{11}/H_{22}$$

where $w = R_1/R_2$ and $t = H_{11}/H_{22}$.

4.4 INTENSITY AND PHASE ICM SAR

This option calculates both the ML and ICM classification, using a multilook intensity image R_i and a phase difference Y. The input data for this processing are two multilook bands R_i and R_j, and the corresponding multilook complex image $R_{ij}^{(n)}$ (see **eq. (6)**).

The rest of the process is as presented in previous sections, namely for classification using a pair of intensities.

In order to derive the joint density of R_1 and Y, intensity and phase difference data obtained from two components S_i and S_j of the scattering matrix, consider the image

$$B_1 = \frac{nR_1}{H_{11}} = \frac{\sum_{k=1}^{n} |S_i(k)|^2}{H_{11}}$$

The joint density of B_1 and Y is given by

$$p(B_1,y) = \frac{B_1^{n-1}\exp\left(-\dfrac{B_1}{1-|r_c|^2}\right)}{2\,p\,\Gamma(n)} {}_1F_1\left[1;\; \frac{1}{2};\; \frac{b^2}{1-|r_c|^2}\, B_1\right] + \frac{b\, B_1^{n-\frac{1}{2}}\exp\left(-\dfrac{B_1(1-b^2)}{1-|r_c|^2}\right)}{2\,p\,\Gamma(n)\sqrt{1-|r_c|^2}}$$

where ${}_1F_1$ is the Confluent hypergeometric function (Abramowitz and Stegun, 1964).

5 EXPERIMENTAL RESULTS

In Correia (1998) applications of all the aforementioned classifications are presented, aiming at the assessment of the feasibility of the proposed system and methodology.

The results here presented are obtained using a space shuttle SIR-C/X-SAR image, bands L and C, type MLC (Multi-Look Complex), with 4.7854018 as its nominal number of looks. Its pixel spacing is of 12.5×12.5 meters. It was obtained the 14^{th} of April, 1996, over the region of Petrolina, PE, Brazil, an agricultural area exhibiting several crops. The image has 407x370 pixels, and was taken at 09°07' S, 40°18' W.

The classes of interest for this study are river (blue), caatinga (green), prepared soil (red), soy (magenta), tillage (cyan) and corn (yellow). Samples of each class were obtained, of sizes 4949, 5177, 3221, 2609, 635 and 3505, respectively.

Figure 5 shows two colour composites of the original data. To the right, C-band data is shown with the HH polarisation in the red channel, the HV in the green and the VV in the blue. To the left, L-band with the same colour coding. FIG. 5

The equivalent number of looks (ENL) was estimated as 2.97479. This value is the mean of the ENLs for each component, as presented in **Table 1**. As expected, this value is below the nominal number of looks due to, among other factors, the lack of independence between individual elements in **eq. (3)**.

TABLE 1 - ESTIMATED ENLs FOR ALL THE AVAILABLE BANDS AND POLARISATION, AND OVERALL MEAN

	Band	
Polarisation	**L**	**C**
HH	2.6688	2.67133
HV	3.18357	2.97230
VV	3.53396	2.81879
Mean	2.97479	

Large samples were collected over homogeneous areas, in order to be able to apply a decorrelation algorithm. This method first estimates the autocorrelation function, in order to define the most suited lags for subsampling in both horizontal and vertical directions. All samples passed the c^2 goodness of fit test at the 1% level of significance, revealing no significant departure from the hypothesised distribution.

All four types of classifications were obtained, and the best one, for both L and C bands, was obtained when two intensity images were used. In particular, the pairs HV-VV and HH-HV were the most successful in bands L and C, respectively, for either ML or ICM classifications.

The comparison among classifications was performed using the coefficient of agreement k, in order to assess quantitatively the significance of the differences. Using this criterion, for the considered image it was possible to conclude that

1) In band L, with intensity pair HV-VV, the ML (ICM, respectively) classification performed, in mean, 111.09% (67.22%, resp.) better than the other classifications.

2) In band C, with the intensity pair HH-HV, the ML (ICM, resp.) classification performed, in mean, 246.95% (180.04%, resp.) better than the other classifications.

Table 2 presents the estimated coefficients of agreement ($\hat{k}$) and their sample variances ($\hat{s}_k^2$) for the best classifications obtained using band C and L intensity pairs, and both ML and ICM algorithms. The sample sizes used to calculate the values presented in **Table 2** are 3844 (river), 3585 (caatinga), 2101 (prepared soil), 2128 (soy), 360 (tillage) and 1946 (corn).

In this way, it can be concluded that, for the current SIR-C image in intensity pairs:

1) The ICM applied to the L band yields to results 28.14% better than the ML, both using the HV-VV components.
2) The ICM applied to the C band yields to results 20.38% better than the ML, both using the HH-HV components.

TABLE 2 - ESTIMATED COEFFICIENTS OF AGREEMENT ($\hat{k}$) AND THEIR SAMPLE VARIANCE ($\hat{s}_k^2$) FOR ALL THE INTENSITY PAIRS CLASSIFICATIONS.

Image	$\hat{k}$	$\hat{s}_k^2 (\times 10^{-5})$
ML – L – HV-VV	0.606424	2.35719
ML – C – HH-HV	0.575344	2.50954
ICM - L – HV-VV	0.777114	1.64955
ICM – C – HH-HV	0.692635	2.10982

Figure 6 shows the best results of the ML classifications for the L (left) and C (right) bands data, when using two intensity images. **Figure 7** shows the best results of the ICM classifications, when using the same bands data. From these figures and from **Table 2** it is possible to conclude that the ICM classification scheme is superior to the ML.

FIG. 6

FIG. 7

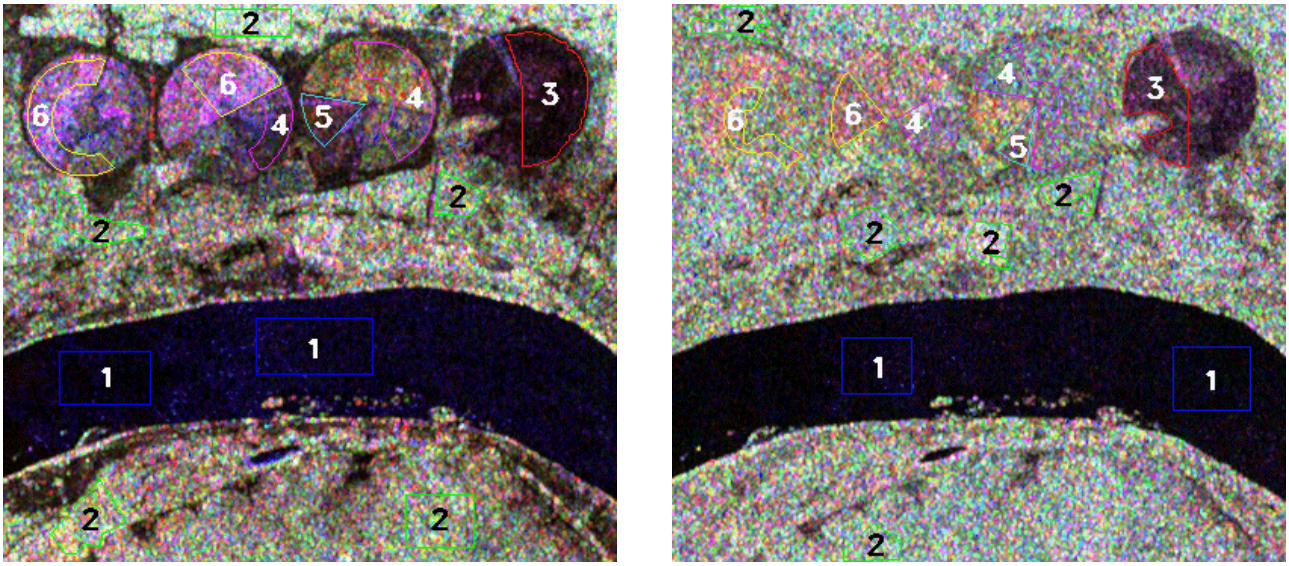

Figure 5 - Two colour compositions of the original data R-HH, G-HV, B-VV, bands L (l) with training sets and C (r) with test sets.

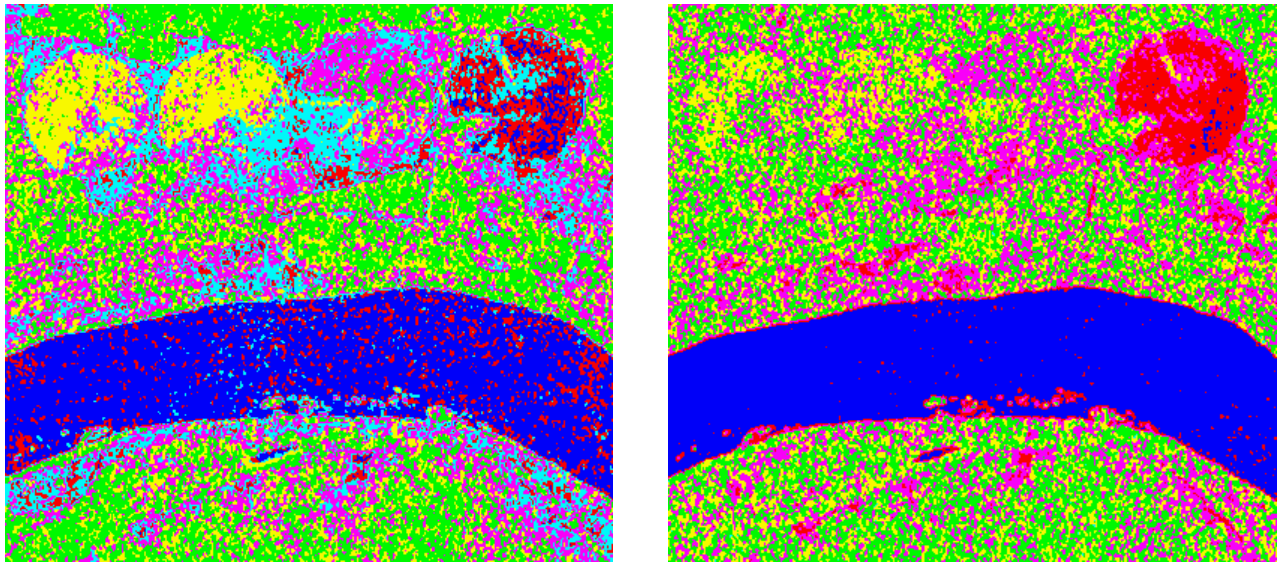

Figure 6 - ML classifications of the L (left, using HV and VV components) and C (right, using HH and HV components) data sets.

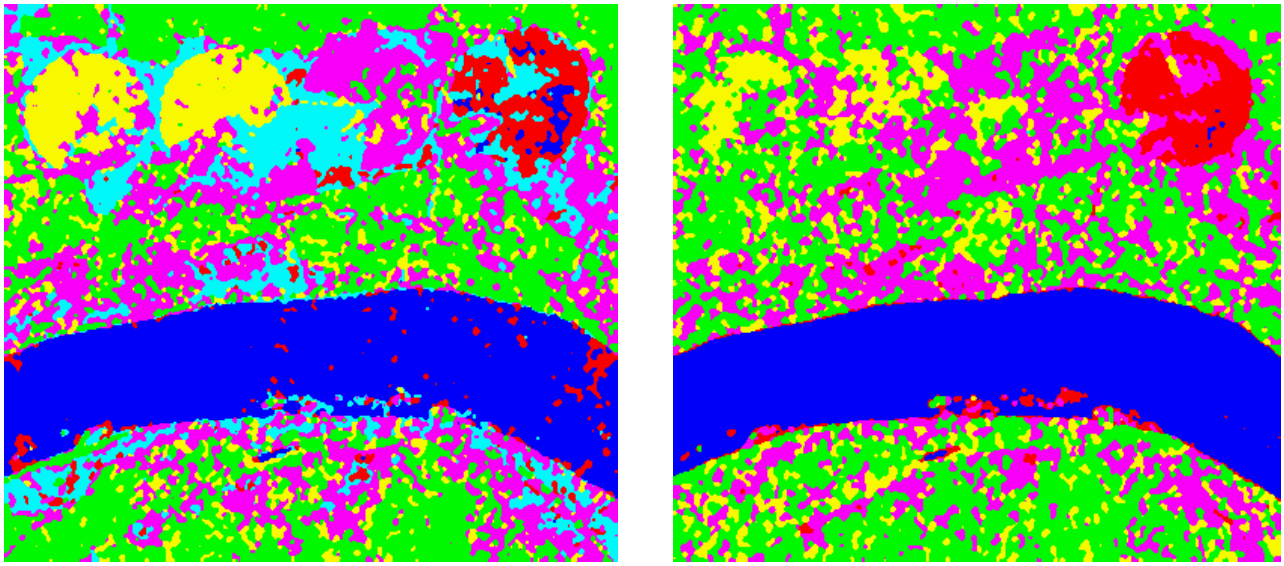

Figure 7 - ICM classifications of the L (left, using HV and VV components) and C (right, using HH and HV components) data sets.

6 CONCLUSIONS

In this paper a system for pointwise and contextual polarimetric multilook SAR image classification was presented. It functions as and add-in to the ENVI system, and it was developed in IDL. The system was built with the interactivity and user-friendliness in mind. It is also goal-driven, so users not familiar to it can learn it easily.

The system proved being efficient for the classification of a SIR-C/X-SAR image, though the modelling of data from all the observed classes was restricted, in the sense that only a model for homogeneous areas was considered.

According to Landis and Koch (1977), the classifications obtained with this system qualify as "very good", using the coefficient of agreement k as a measure of quality.

For the considered data, the use of contextual information (incorporated through the ICM classification algorithm) yields to a significant classification improvement, of the order of 24%. This improvement is not so dramatic as those obtained for single band amplitude data (Vieira, 1996), which is a somewhat expected result due to the larger amount of information potentially present in polarimetric data sets.

REFERENCES

Abramowitz, M.; Stegun, I. *Handbook of mathematical functions: with formulas, graphs, and mathematical tables.* New York, Dover, 1964.

Correia, A.H. *Desenvolvimento de classificadores de máxima verossimilhança e ICM para imagens SAR polarimétricas*. (MSc in Remote Sensing) – Instituto Nacional de Pesquisas Espaciais. São José dos Campos, SP, Brazil, 1998. To be presented.

DeGrandi, G.; Lemoine, G.; Sieber, A. Supervised fully polarimetric classification: an experimental study on the MAESTRO-1 Freiburg data set. In: IGARSS'92 International Geoscience and Remote Sensing Symposium'92, Houston, May. 26-29, 1992. *International Space Year: space remote sensing*. IEEE, 1992. v. I, p. 782–785.

DeGroot, M.H. *Probability and statistics***.** Menlo Park, Addison-Wesley, 1975. 607 p.

Du, L.J.; Lee, J.S. Polarimetric SAR image classification based on target decomposition theorem and complex Wishart distribution. In: IGARSS'96 International Geoscience and Remote Sensing Symposium'96, Lincoln, May. 27-31, 1996. *Remote Sensing for a Sustainable Future*. IEEE, 1996. v. I, p. 439–441.

Frery, A.C.; Müller, H.J.; Yanasse, C.C.F; Sant'Anna, S.J.S. A model for extremely heterogeneous clutter. *IEEE Trans. Geosc. Rem. Sens.*, 35(3):1–12, 1997a.

Frery, A.C.; Yanasse, C.C.F.; Vieira, P.R.; Sant'Anna, S.J.S.; Rennó, C.D. A user-friendly system for synthetic aperture radar image classification based on grayscale distributional properties and context. Simpósio Brasileiro de Computação Gráfica e Processamento de Imagens, 10., 1997, p. 211–218. *SIBGRAPI 97*. Los Alamitos, CA, IEEE Computer Society, 1997b.

Goodman, N. R. Statistical analysis based on a certain multivariate complex Gaussian distribution. *Ann. Math. Stat.*, 34(1):152–177, 1963.

Kong, J.A. Identification of terrain cover using the optimal polarimetric classifier. *J. Electrom. Waves Appl.***,** 2(2):171–194, 1988.

Landis, J.; Koch, G.G. The measurements of observer agreement for categorical data. *Biometrics*, 33(3):159–174, 1977.

Lee, J.S.; Hoppel, K.W.; Mango, S.A. Intensity and phase statistics of multi-look polarimetric and interferometric SAR imagery. *IEEE Trans. Geosc. Rem. Sens,*. 32(5):1017–1028, 1994.

Lee, J.S.; Du, L.; Schuler, D.L.; Grunes, M.R. Statistical analysis and segmentation of multi-look SAR imagery using partial polarimetric data. In: IGARSS'95 International Geoscience and Remote Sensing Symposium'95, Firenze, Jul. 10–14, 1995. *Quantitative Remote Sensing for Science and Applications*. Piscataway, IEEE, 1995. v. III, p. 1422–1424.

Lee, J.S.; Grunes, M.R. Classification of multilook polarimetric SAR imagery based on complex Wishart distribution. *Int. J. Rem. Sens*., 15(11):2299–2311, 1994.

Lim, H.H; Swartz, A.A.; Yueh, H.A.; Kong, J.A.; Shin, R.T.; Van Zyl, J.J. Classifications of earth terrain using polarimetric SAR images. *J. Geophys. Res.*, 94(B6):7049–7057, 1989.

Nezry, E.; Lopés, A.; Ducrot-Gambart, D.; Nezry, C.; Lee, J.S. Supervised classification of K-distributed SAR images of natural targets and probability of error estimation. *IEEE Trans. Geosc. Rem. Sens.*, 34(5):1233–1242, 1996.

Quegan, S.; Rhodes, I. Statistical models for polarimetric data: consequences, testing and validity. *Int. J. Rem. Sens.*, 16(7):1183–1210, 1995.

Sarabandi, K. Derivations of phase statistics from the Mueller matrix. *Radio Science*, 27(5):553-560, 1992.

Srivastava, M.S. On the complex Wishart distribution. *Ann. Math. Stat.*, 36(1):313–315, 1963.

Tur, M.; Chin, K.C.; Goodman, J.W. When is speckle noise multiplicative? *Appl. Opt.*, 21:1157–1159, 1982.

Ulaby, F. T.; Elachi, C. *Radar polarimetric for geoscience applications.* Norwood, Artech House, 1990. 364p.

Vieira, P.R. *Desenvolvimento de classificadores de maxima verossimilhança e ICM para imagens SAR*. (MSc in Remote Sensing) – Instituto de Nacional de Pesquisas Espaciais. São José dos Campos, SP, Brazil, 1996. 251 p. (INPE-6124-TDI/585).

Vieira, P.R.; Yanasse, C.C.F.; Frery, A.C; Sant'Anna, S.J.S. Um sistema de análise e classificação estatísticas para imagens SAR. In: Primeras Jornadas Latinoamericanas de Percepción Remota por Radar, Buenos Aires, Dez. 1996. *Técnicas de Processamiento de Imágenes*. Paris, ESA, 1996. p. 170–185.

Yueh, S.H.; Kong, J.A.; Jao, J.K.; Shin, R.T.; Novak, L.M. K-distributition and polarimetric terrain radar clustter. *J. Electrom. Waves Appl.*, 3(8):747–768, 1989.